Availability and Interpretability of Optimal Control for Criticality Estimation in Vehicle Active Safety

Stephan Herrmann and Wolfgang Utschick
Technische Universität München, Munich, Germany, Email: {s.herrmann,utschick}@tum.de

***Abstract*—Current and future vehicular active safety systems rely on situation interpretation algorithms for mapping sensor information of the environment to a criticality or threat value. In dangerous driving situations, these metrics are used to trigger a range of safety interventions from warning the driver, pre-tensioning of the braking system, automatic emergency braking, and automatic emergency braking and steering. For highly complex functions like automatic braking and steering, validation through real-world test drives become increasingly costly and time-consuming. Here, simulation studies can be used, where a large set of dangerous driving scenarios is labeled with a reference criticality, that should represent the *true* criticality. In order to find such a ground truth criticality, we propose an optimal control formulation of criticality taking into account a vehicle dynamics model as well as lane constraints. Further, using stochastically generated driving scenes, we explore the trade-off between different goal functions and constraint formulations for interpretability and convergence of the criticality measure in simulation scenarios.**

I. Introduction

Vehicle active safety systems (ASS) use sensors like radar and video cameras to analyze the surroundings of the host vehicle for imminent collision threats. Situation interpretation algorithms then estimate a threat metric based on the environment perception, i.e., a value c between zero and one, which we refer to as *criticality*. Informally, a criticality value of $c = 0$ corresponds to the complete absence of danger for the host vehicle or other traffic participants and $c = 1$ indicates that a collision is unavoidable. In a dangerous driving situation, e.g., a rear-end collision scenario due to driver inattentiveness, ASS use the criticality to trigger a series of automatic interventions from audiovisual and haptic warnings, to pre-tensioning of the braking system, up to automatic emergency braking [1].

Future ASS and driver assistance systems hold the potential to further decrease the number of traffic accidents by executing automatic lateral evasion maneuvers for collision avoidance [2], [3]. Due to the ever increasing number of sensor information and complexity of safety functions, the parameterization and performance evaluation of real-time capable situation interpretation algorithms has become an important bottleneck for the validation of current and future safety systems in series production vehicles [4]. This validation has to show that the ASS is well-behaved, i.e., it reduces traffic accidents as much as possible without intervening in driving situations where no intervention is necessary (so called *false-positive* interventions). Simulation studies are increasingly used as tools in the development process, e.g., for parameter tuning [5], [6], to estimate the performance of real-time capable situation interpretation algorithms [7], to specify sensor requirements [8], and for generating reference data sets for the training of fast criticality classifiers [9], [10]. These applications of simulation studies have in common that they require a definition of a reference criticality, which specifies the *true* threat of a traffic scene. To serve as reference values, such nominal criticality labels should be computed with a focus on a precise domain modeling instead of a focus on real-time capability.

In [10], optimal control has been used for this labeling task to generate a reference data set for lateral evasion by braking and steering. The appeal of an optimal control formulation of the nominal criticality is that, first, a vehicle model for the host vehicle can be enforced in the form of a differential equation. This enables a realistic simulation of the vehicle behavior for a prediction horizon of a few seconds of the highly nonlinear dynamics of emergency evasion maneuvers. Second, information about the environment like lane boundaries and moving obstacles can be taken into account in the form of lane keeping and collision avoidance constraints.

In this contribution we expand upon the work in [10] by analyzing the trade-off between the *interpretability* and *availability* of criticality measures based on optimal control. We refer to the interpretability as the degree of difficulty of relating the optimal value of an optimal control problem to the ability, skill, or attention level of the vehicle driver. For given set of driving scenes, we designate the availability of an OCP as the fraction of driving scenes for which a solution of the OCP can by found using a numerical solver.

In Section II, we discuss optimal control problems with varying actor constraints and goal functions to explore the trade-off between model precision, interpretability, and the ability to find evasion trajectories. In order to generate a data set of driving scenes and criticality values, we propose a probabilistic sampling scheme in Section III. In Section IV, this data set is used to quantify the availability of the proposed OCP formulations using a stochastically generated scene set.

II. Reference Criticality from Optimal Control

The problem of finding evasion trajectories has been treated as an optimal control problem in, e.g., [11], [3], [12]. We consider the case of longitudinal traffic on a straight lane with widths of the left and right lanes B_l, B_r. The dynamics of the host vehicle are modeled using a nonlinear single-track model with the state vector

$$\mathbf{s} = \begin{bmatrix} x & y & v & \beta & \psi & \omega & \delta & F \end{bmatrix}^\mathrm{T}, \tag{1}$$

where $x,\ y$ are the Cartesian coordinates of the host vehicle in an inertial coordinate system attached to the road surface, v is the velocity of the center of gravity (COG), β is the body slip angle, $\psi,\ \omega$ are the yaw angle and rate, δ is the steering angle

978-3-9815370-6-2/DATE16/ ©2016 EDAA

of the front wheel, and F_{tot} is the total tangential tire force. The tangential tire force is distributed between the tangential tire forces of the front and rear wheels:

$$F_{\text{tf}} = 0.6F, \quad F_{\text{tr}} = 0.4F. \tag{2}$$

In Sections II-B and II-C, we discuss the modeling of the tire side forces F_{sf}, F_{sr}.

The dynamics of the host vehicle are governed by a nonlinear ordinary differential equation which we note for completeness, referring to [13] for a derivation:

$$\begin{bmatrix} \dot{x} \\ \dot{y} \\ \dot{v} \\ \dot{\beta} \\ \dot{\psi} \\ \dot{\omega} \\ \dot{\delta} \\ \dot{F}_{\text{tot}} \end{bmatrix} = \begin{bmatrix} v\cos(\psi+\beta) \\ v\sin(\psi+\beta) \\ a_{\text{lon}} \\ a_{\text{lat}}/v - \omega \\ \omega \\ \frac{1}{I}(F_{\text{sf}}\cos(\delta)l_f + F_{\text{tf}}\sin(\delta)l_f - F_{\text{sr}}l_r) \\ u_1 \\ u_2 \end{bmatrix}, \tag{3}$$

where the rates of change of the total tangential tire force and of the front wheel steering angle are used as control inputs

$$\mathbf{u} = \begin{bmatrix} u_1 & u_2 \end{bmatrix}^{\text{T}}. \tag{4}$$

The longitudinal and lateral accelerations at the COG are

$$\begin{aligned} a_{\text{lon}} = \frac{1}{m}\,&(F_{\text{tr}}\cos(\beta) + F_{\text{tf}}\cos(\delta-\beta) \\ &+F_{\text{sr}}\sin(\beta) - F_{\text{sf}}\sin(\delta-\beta)), \end{aligned} \tag{5}$$

$$\begin{aligned} a_{\text{lat}} = \frac{1}{m}\,&(-F_{\text{tr}}\sin(\beta) + F_{\text{tf}}\sin(\delta-\beta) \\ &+F_{\text{sr}}\cos(\beta) + F_{\text{sf}}\cos(\delta-\beta)). \end{aligned} \tag{6}$$

In this model, m is the vehicle mass, I is the moment of intertia, and l_f, l_r are the distances of the front and rear wheel from the COG as given in Table I. In the remainder, we use the shorthand $\dot{\mathbf{s}} = f(\mathbf{s}, \mathbf{u})$ for the vehicle dynamics.

The longitudinal and lateral accelerations a_{lon}, a_{lat} at the COG, as well as the front and rear tire tangential forces F_{tf}, F_{tr} and tire side forces $F_{\text{sf}}, F_{\text{sr}}$ are illustrated in Figure 1.

TABLE I. PARAMETERS FOR THE SINGLE-TRACK MODEL (3).

parameter	symbol	value	unit
mass	m	1450	kg
moment of inertia	I	1920	kgm^2
COG distance from front wheel	l_f	1.3	m
COG distance from rear wheel	l_r	1.45	m
host vehicle body length	L	5.1	m
host vehicle body width	W	2.1	m
stiffness factor	B	0.239	$1/^\circ$
shape factor	C	1.19	1
curvature factor	E	-0.678	1

We assume that the host vehicle is in a state of stationary lane following at the start of the evasion maneuver, which is valid, e.g., when the driver of the host vehicle is passive or inattentive. This choice reduces the number of values necessary to specify a driving scene, since we can set the initial states

$$\psi_0 = 0, \quad \omega_0 = 0, \quad \beta_0 = 0, \quad F_0 = 0, \quad \delta_0 = 0. \tag{7}$$

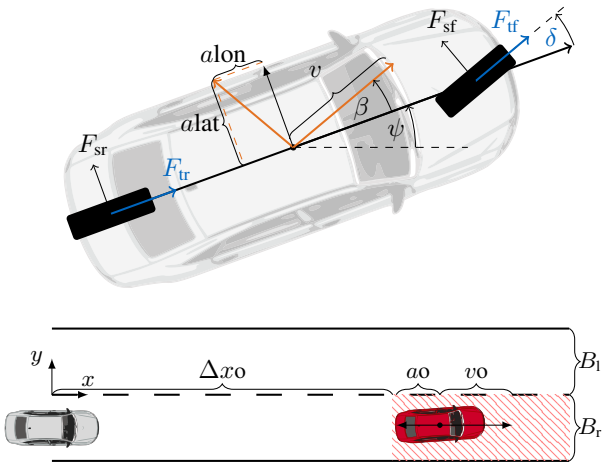

Fig. 1. Top: states of the single-track model, bottom: road geometry, host vehicle (gray), obstacle (red) states, and restricted area (dashed).

We assume that an obstacle is situated in front of the vehicle, e.g., another car or a bicycle. This obstacle is defined by its distance from the host vehicle Δx_{o}, its speed v_{o} and longitudinal acceleration a_{o}. For the duration T of the prediction horizon, the position of the obstacle is predicted using the assumption that the obstacles acceleration remains constant as long as its velocity is greater than zero and that it follows the lane.

We model a lane changing maneuver with braking and steering where we assume that the host vehicle has to change to the adjacent lane. The host vehicle has to stay clear of a restricted area starting from the rear-end of the obstacle and covering the occupied lane. Note that this forbidden area changes over time as the obstacle moves forward. See Figure 1 for an illustration of the scene model and host vehicle states.

Under these assumptions, a driving scene is defined by the initial speed of the host vehicle v_0, its initial lateral offset with respect to the inertial coordinate system y_0, the lane widths B_{l}, B_{r} and the obstacle states.

The underlying principle of criticality labeling based on optimal control is to find a collision-free evasion trajectory for a prediction horizon T that satisfies the vehicle model equations, does not steer of the road, and minimizes the maximum dynamics of the host vehicle, c.f. [11], [3]. This evasion trajectory should minimize a criticality function $f_{\text{crit}}(\mathbf{s}(\cdot), \mathbf{u}(\cdot))$ that maps the vehicle states and control inputs to a criticality.

In the following, we specify a driving scene configuration by a scene vector

$$\mathbf{x} = \begin{bmatrix} y_0 & v_0 & \Delta x_{\text{o}} & v_{\text{o}} & a_{\text{o}} & B_{\text{l}} & B_{\text{r}} \end{bmatrix}^{\text{T}}. \tag{8}$$

Formally, the criticality label $c(\mathbf{x})$ of a scene $\mathbf{x}$ is the optimal value of the following optimal control problem:

$$c(\mathbf{x}) = \min_{\mathbf{s}(\cdot),\mathbf{u}(\cdot)} f_{\text{crit}}(\mathbf{s}(\cdot),\mathbf{u}(\cdot)), \tag{9}$$

$$\mathbf{s}(0) - \mathbf{s}_0 = \mathbf{0}, \tag{a}$$

$$y(T) \geq 0.5W, \tag{b}$$

$$|\psi(T)| \leq \psi_{\text{end}}, \tag{c}$$

$$\dot{\mathbf{s}}(t) - f(\mathbf{s}(t),\mathbf{u}(t)) = \mathbf{0}, \tag{d}$$

$$0.5W - B_{\text{r}} \leq y(t) \leq B_{\text{l}} - 0.5W, \tag{e}$$

$$\mathcal{A}_{\text{o}}(t) \cap \mathcal{A}_{\text{h}}(t) = \emptyset, \tag{f}$$

$$|\delta(t)| \leq \delta_{\max}, \tag{g}$$

$$|u_1(t)| \leq u_{\dot{\delta},\max}, \tag{h}$$

$$u_{\dot{F},\min} \leq u_2(t) \leq 0, \quad \forall t \in [0,T], \tag{i}$$

which we explain in the following. Initial and final state constraints and the ordinary differential equation constraint for the vehicle model are imposed by (a)-(d). The initial state $\mathbf{s}_0$ is given by the entries of the scene vector (8) and the stationary initial conditions in (7). The final state constraint (b) ensures that a lane change maneuver is found by require a minimal lateral offset of half the vehicle width W at the end of the prediction horizon T. To obtain a degree of safety after the completion of the maneuver, the final state constraint on the yaw angle (c) enforces that the angle between the longitudinal axis of the host vehicle deviates from the lane direction by a maximum of $\psi_{\text{end}} = 15°$. The constraint (e) enforces that the host vehicle body stays within the lane boundaries with a safety margin. The lane keeping of the host vehicle is enforced through (e). For a formulation of the lane keeping constraint for clothoidal lanes, see [10].

The anti-collision constraint (f) requires that the area covered by the host vehicle body $\mathcal{A}_{\text{h}}(t)$ never overlaps with the area that is occupied by the obstacle $\mathcal{A}_{\text{o}}(t)$, c.f. Figure 1. Defining the host vehicle body area and the restricted area as convex polytopes with corner coordinates $\mathbf{r}_i(t),\ \mathbf{r}_j(t)$, $i,j = 1,\dots,4$, the anti-collision constraint can be written in terms of a separating hyperplane given by an angle $\phi(t)$ and an offset $b(t)$ that change over time and are added to the OCP (9) as auxiliary variables [10]:

$$[\cos(\phi) \quad \sin(\phi)]^{\text{T}} = \mathbf{n}(t), \tag{10}$$

$$\mathbf{n}^{\text{T}}\mathbf{r}_{\text{i}}(t) \leq b(t)\ \forall i, \tag{11}$$

$$\mathbf{n}^{\text{T}}\mathbf{r}_{\text{o},j}(t) \geq b(t)\ \forall j,\ \forall t \in [0,T]. \tag{12}$$

The actor constraints in (g)-(h) limit the steering angle to $\delta_{\max} = 50°$ and the control inputs to $u_{\dot{\delta},\max},\ u_{\dot{F},\max}$, respectively. The choice of these control bounds is discussed in the following sections.

Note that this OCP formulation can also be used for criticality estimation for lateral evasion inside the host vehicle lane by an appropriate choice of the widths $B_{\text{r}},\ B_{\text{l}}$.

A. Interpretability and Availability of the OCP

The choice of the criticality function $f_{\text{crit}}(\mathbf{s}(\cdot),\mathbf{u}(\cdot))$ as well as the choice of the control bounds $u_{\dot{\delta},\max},\ u_{\dot{F},\max}$ and the tire model have a significant influence on the interpretability of the criticality function and on the difficulty of solving the OCP (9) using optimization codes. Imposing strict constraints on the change rates of the actors (i.e., braking and steering) leads to a realistic model of the cars behavior even at the limits of maneuverability. Thus, imposing these actor constraints improves the interpretability of the obtained trajectories. However, when a high number of explicit constraints is enforced in the OCP, highly dangerous situations can possibly not be labeled, since no feasible solution to the evasion problem can be found by a numerical solver. First, this can be caused the the physical limits of the vehicle due the actor speed and limited tire friction, such that an evasion trajectory satisfying all constraints may simply not exist. A second reason for the inability to solve an OCP is due to the fact that the numerical optimal control solvers used, e.g., in [11], [3], [12] and in this work, require an initial guess for the evasion trajectory, which can influence the ability of the solver to find a solution since they are not globally convergent.

When generating a large data set $\{\mathbf{x}_i, c(\mathbf{x}_i)\}_{i=1,\dots,N}$ of N pairs of scenes and criticalities, we want to be able to assign a label to as many scenes $\mathbf{x}_i$ as possible, even if a collision cannot be avoided for a given scene configuration. Hence, there has to be a trade-off between this availability requirement and the desire to enforce realistic actor constraints. In the following, we discuss three possible combinations of goal function, actor constraints and tire model.

B. Max-norm acceleration, input constraints, and tire model

In this version of the criticality OCP, the max-norm of the acceleration vector at the COG of the host vehicle is used in the cost function (9), i.e.,

$$\mathbf{a}(t) = [a_{\text{lon}}(t) \quad a_{\text{lat}}(t)]^{\text{T}},$$
$$f_{\text{crit}}(\mathbf{s}(\cdot),\mathbf{u}(\cdot)) = \max_{t\in[0,T]} \frac{\|\mathbf{a}(t)\|_2}{\mu g}, \tag{13}$$

where μ is the road friction coefficient and $g = 9.81\text{m/s}^2$ is the gravitational constant. With this goal function of the OCP, we can find evasion trajectories with minimal max-norm of the acceleration, which are easily interpretable: given such a trajectory, we can reason about whether the driver is capable of performing a maneuver with at least as much acceleration. Also, the minmax acceleration can be related to an estimate of the friction coefficient of the road surface in order to determine if the evasion maneuver is physically possible. An alternative to the acceleration norm is the norm of the tire force at the front wheel as used in [3].

The tire forces are modeled using the *magic formula* tire model [14] and a simple coupling of tangential and side forces. In the single-track vehicle model, the side slip angles of the front and rear wheels are given as [13]

$$\alpha_{\text{f}} = \delta - \arctan\left(\frac{l_f\omega + v\sin(\beta)}{v\cos(\beta)}\right), \tag{14}$$

$$\alpha_{\text{r}} = \arctan\left(\frac{l_r\omega - v\sin(\beta)}{v\cos(\beta)}\right). \tag{15}$$

Denoting the rear and front tires with subscripts $_{\text{r,f}}$, the tire side forces are approximated by the magic formula [14]

$$f_{\text{s,f/r}}(\alpha) = \mu F_{\text{z,f/r}} \sin\left(C\arctan(\Phi_{\text{f/r}})\right), \tag{16}$$
$$\Phi_{\text{f/r}} = B\alpha_{\text{f/r}} - E(B\alpha_{\text{f/r}} - \arctan(B\alpha_{\text{f/r}})),$$

with the normal forces on the tires given as

$$F_{\text{z,f/r}} = mg\frac{l_{\text{r/f}}}{l_{\text{r}} + l_{\text{f}}}. \tag{17}$$

Refer to Table I for the values of the shape parameters B, C, E. The tire forces are constrained by an upper and lower bound on the total braking force and a coupling of the tangential and side forces via the constraints

$$\begin{aligned} -\mu mg \leq F_{\text{tot}}(t) \leq 0, \\ F_{\text{s,f/r}}(\alpha(t), F_{\text{tf}}(t)) = f_{\text{s,f/r}}\sqrt{1 - \left(\frac{F_{\text{t,f/r}}(t)}{\mu F_{\text{z,f/r}}}\right)^2}, \end{aligned} \tag{18}$$

which ensures that the tire force vectors at the front and rear wheels lie within a force ellipse [15].

For the control bounds, we choose

$$u_{\dot{\delta},\text{max}} = \frac{2\pi}{15}, \quad u_{\dot{F},\text{min}} = \frac{gm}{0.2}, \tag{19}$$

which corresponds to one turn of the steering wheel per second with a steering ratio of 15 and a ramp-up time of the full braking force of gm in 200 milliseconds. These choices of control constraints are done by rule of thumb and, in practice, depends on the host vehicle and the assumed driver capabilities.

C. Max-norm acceleration, input constraints, and linear tire

The tire model as expressed in (16) correctly captures the fact that the force generated by a tire is limited by the friction coefficient of the road surface and the weight of the vehicle. A relaxation of this model is the use of a linear tire model

$$F_{\text{s,f/r}}(\alpha_{\text{f/r}}) = k_{\text{f/r}}\alpha_{\text{f/r}}, \quad k_{\text{f/r}} = \mu F_{\text{z,f/r}} BC \tag{20}$$

where $k_{\text{f/r}}$ is the cornering stiffness of the front and rear tire, respectively, and is equal to the slope of (16) at $\alpha_{\text{f/r}} = 0$ [14].

Evidently, the linear tire model can result in tire forces that are higher than physically possible given the vehicle weight and the road friction coefficient. Nevertheless, when the linear tire model is combined with the max-norm of the acceleration vector (13) as the goal function, the optimal trajectories will inherently use the least amount of peak-acceleration and thus also minimize the peak-force at the COG. When an evasion trajectory for a scene $\mathbf{x}$ features a peak-acceleration that is higher than would be physically possible, we have still obtained a criticality label $c(\mathbf{x}) > 1$, which is a lot more useful than not finding a solution at all.

D. Max-norm of maximum dynamics without input constraints

To further decrease the number of constraints imposed on the dynamics of the host vehicle without sacrificing interpretability, we remove the rate constraints (h) and (i). In order to still find realistic evasion trajectories, we propose to use a goal function that simultaneously minimizes the maximum acceleration, the maximum steering rate u_1, and maximum braking force rate u_2, i.e.,

$$\begin{aligned} f_{\text{crit}}(\mathbf{s}(\cdot), \mathbf{u}(\cdot)) = \max_{t\in[0,T]} \max\Bigg\{ &\frac{\|\mathbf{a}(t)\|_2}{\mu g}, \\ &\frac{|u_1(t)|}{u_{\dot{\delta},\text{max}}}, \frac{|u_2(t)|}{u_{\dot{F},\text{max}}} \Bigg\}, \end{aligned} \tag{21}$$

which is inspired by the cost function used in [16]. Note that the three dynamic properties are arguments of the $\max$ function and are weighted by their physical bounds. This goal function can be interpreted as follows: if we are able to find an evasion trajectory $\mathbf{s}(\cdot), \mathbf{u}(\cdot)$ with $f_{\text{crit}}(\mathbf{s}(\cdot), \mathbf{u}(\cdot)) \leq 1$, we know that the peak-acceleration of the trajectory can be supported by the road surface and that the rates of change of the controls can be executed by the steering and braking actors. On the other hand, if $f_{\text{crit}}(\mathbf{s}(\cdot), \mathbf{u}(\cdot)) > 1$, we know that at least one physical constraint is violated, i.e., the collision cannot be avoided. In conclusion, while the criticality function (21) is more complex than the max-norm function criticality (13), it still indicates the degree of feasibility of collision avoidance and allows to relax the control constraints.

Numerical solution

To compute solutions of the OCP (9), we employ the direct multiple shooting method [17] using the CasADi [18] library for optimal control and automatic differentiation together with the interior point solver IPOPT [19]. For details on the numerical solution approach, see [10].

III. Sampling of critical driving scenes

For the creation of synthetic data sets of driving scenes and associated evasion trajectories and criticalities, we specify a probabilistic model of the a-priori distribution of driving scenes. For simplicity, we fix the lane width to

$$B_{\text{r}} = B_{\text{l}} = 4\text{m}. \tag{22}$$

We investigate a velocity range between $v_{\text{min}} = 4\text{m/s}$ and $v_{\text{max}} = 30\text{m/s}$ and choose the upper and lower bounds for the initial lateral offset as

$$y_{\text{min}} = -B_{\text{r}} + 0.5W, \quad y_{\text{max}} = -0.5W, \tag{23}$$

which ensures that the host vehicle starts on on the right lane. With a straight lane model and the assumption that the obstacle always occupies the same lane as the host vehicle, the scenario is symmetric in the lateral offset of the host vehicle. Therefore, it is sufficient to simulate only scenes with $y_0 \leq 0$. As illustrated in Figure 1, we locate the inertial coordinate system at the projection of the host vehicle position onto the center line of the road. With this choice, the initial x is always equal to zero. As the upper and lower bounds for the obstacle acceleration, we chose $a_{\text{min}} = -6\text{m/s}^2$, $a_{\text{max}} = 0\text{m/s}^2$.

To generate stochastic samples of the remaining entries of the scene configuration in (8), we specify a probabilistic model for those entries. This model should lead to a high frequency of critical scenes while at the same time covering the range of desired host vehicle velocities, lateral offsets, and obstacle decelerations. To this end, we designate the host vehicle velocity, offset, and obstacle deceleration as independent variables and draw independent and identically distributed (i.i.d) samples

$$v_{0,i} \sim \mathcal{U}(v_{\text{min}}, v_{\text{max}}), \tag{24}$$

$$y_{0,i} \sim \mathcal{U}(y_{\text{min}}, y_{\text{max}}) \tag{25}$$

$$a_i \sim \mathcal{U}(a_{\text{min}}, a_{\text{max}}), \tag{26}$$

where $\mathcal{U}(a, b)$ is the uniform distribution on the interval $[a, b]$. The obstacle velocity v_{o} has to be upper-bounded by the host

vehicle velocity v_i to obtain collision scenes. It is modeled as a dependent variable with a uniform probability distribution,

$$v_{\mathrm{o},i} \sim \mathcal{U}(0, v_i). \tag{27}$$

In order to generate dynamic evasion maneuvers, a uniform distribution of the time-to-collision t_{ttc} is used, i.e.,

$$t_{\mathrm{ttc},i} \sim \mathcal{U}(0.5\mathrm{s}, 2\mathrm{s}), \tag{28}$$

which is motivated by the fact that the time to collision is a well studied surrogate value for the criticality of longitudinal traffic [20]. Under the assumption of a constant host vehicle velocity and constant obstacle acceleration, the distance between the host vehicle and obstacle obstacle (neglecting the body length) vanishes at $t = t_{\mathrm{ttc}}$, i.e.,

$$0 = x_{\mathrm{o}} + (v_{\mathrm{o}} - v)t_{\mathrm{ttc}} + 0.5a_{\mathrm{o}}t_{\mathrm{ttc}}^2, \tag{29}$$

which we can solve for the distance of the obstacle,

$$x_{\mathrm{o}} = \frac{-2(v_{\mathrm{o}} - v)}{a_{\mathrm{o}}t_{\mathrm{ttc}}}. \tag{30}$$

IV. Numerical Evaluation

For all simulations, the prediction horizon is set to $T = 2.5\mathrm{s}$ and it is discretized into 30 equal-length intervals for numerical simulation and optimization. We assume a road surface with a friction coefficient of $\mu = 1$. In our evaluation, we refer to the OCP with max-norm acceleration cost and nonlinear tire (Section II-B) as MINA-NLT, the linear tire approximation (Section II-C) as MINA-LT, and the OCP with the maximum dynamics cost and unconstrained inputs (Section II-D) as MINDYN-LT.

First, we evaluate the effect of the OCP variants by studying a simple scenario with a standing obstacle. We fix the initial velocity of the host vehicle to $v_0 = 15\mathrm{m/s}$ and the lane widths are fixed to $B_{\mathrm{l}} = B_{\mathrm{r}} = 3.5m$. In Figure 2, the optimized maneuvers for the initial states $v_0 = 15\mathrm{m/s},\ x_{\mathrm{o}} = 16.1\mathrm{m},\ y_{\mathrm{o}} = -2\mathrm{m}$ are illustrated using a top-down view of the evasion maneuvers and a trace plot of the longitudinal and lateral acceleration over time. In the top-down view, we see only a marginal difference between the trajectories found using MINA-NLT and MINA-LT while MINDYN-LT leads to a markedly shorter arc length of the evasion maneuver. The solution of MINDYN-LT (blue curve) has a higher maximum norm of the acceleration vector compared to MINA-(N)LT, which is due to the fact the cost function (21) of MINDYN-LT balances the acceleration norm and actor rates, whereas the cost function (13) of MINA-(N)LT optimizes the max-norm of the acceleration vector. Note that the acceleration for all OCP variants follows a common shape for all OCPs: starting from zero acceleration in point A, the longitudinal and lateral acceleration jointly increase towards point B on to the maximum lateral acceleration at point C. Then, the acceleration vector approximately traverses a semi-circle to achieve the maximum lateral acceleration in the opposite direction at point D to avoid steering off the lane. In Figure 3, we depict the criticality labels obtained for varying initial obstacle distances Δx_{o}, and lateral offset y_{o}. Note that MINDYN-LT can find criticality labels for obstacle distances under 10 meters, whereas MIN-NLT and MINA-LT cease to provide a label for such small distances. All versions of the OCP lead to a smooth criticality estimate for varying obstacle distances and lateral offsets of the host vehicle, which was confirmed for the linear tire model in [10]. For multiple reasons, this smoothness property is important for the application of optimal control solvers as a labeling tool for simulation campaigns. First, it conforms to intuition that the criticality increases smoothly with a decreasing obstacle distance. For higher absolute values of the lateral offset $|y_0|$, the criticality increases since more steering is required to achieve the desired lane change. Second, a smooth criticality value can be more easily approximated by machine learning algorithms [10] or even look-up tables, enabling fast real-time criticality estimation. The criticality curve for the linear tire and unconstrained inputs (blue) has a small dent at around $x = 33\mathrm{m}$, which can be attributed to the fact that the OCP can only be solved to a local optimum.

In order to quantify the availability of the OCP formulations, we use the a-priori distribution of driving scenes derived in Section III to sample $N = 1000$ i.i.d. scene samples with a moving target and varying initial states as a test set. The empirical availability of an OCP is the fraction of the scenes where a a solution to the OCPs was found. In Table II, we list the availability of the OCPs as well as their average run time. For the run time, we not observe any significant difference between the OCP formulations. For the stochastically generated test set, we observe a significant increase of the availability of criticality labels from 89.4% for MINA-NLT, to 94% for MINA-LT, up to 99.4% for the most unconstrained problem MINDYN-LT. These results confirm the observation made in the example scenario of Figure 2, i.e., that the MINA-LT and MINDYN-LT OCPs can provide labels for highly critical scenarios.

TABLE II. Availability and average runtime of criticality OCP formulations for 1000 random scenes.

	MINA-NLT	MINA-LT	MINDYN-LT
availability [%]	89.4	94.0	99.4
avg. run time [s]	51.93	51.91	51.94

V. Conclusion and Outlook

In this study we have compared three optimal control problem formulations for labeling the criticality of lateral evasion maneuvers with braking and steering in longitudinal traffic situations and a moving obstacle. Solving optimal control problems with tire force saturation and actor constraints yields realistic trajectories but also leads to an inability to find evasion trajectories for highly critical driving situations. We have studied this trade-off between realism, interpretability, and the availability of evasion trajectories using stochastically generated driving scenes and were able to confirm that the proposed relaxed OCPs increase the availability at a moderate cost of interpretability. In future work, the presented scene generation and labeling scheme can serve to generate reference data sets to compare the performance of real-time capable criticality estimation algorithms. Another important future application is the approximation of the criticality using regression techniques to achieve a fast situation interpretation. The influence of sensor noise on the accuracy of vehicle trajectories has been studied in [13], [12]. Another important topic would be an investigation of the influence of imperfect information about the host vehicle mass and the center of gravity on the resulting evasion trajectories and criticality.

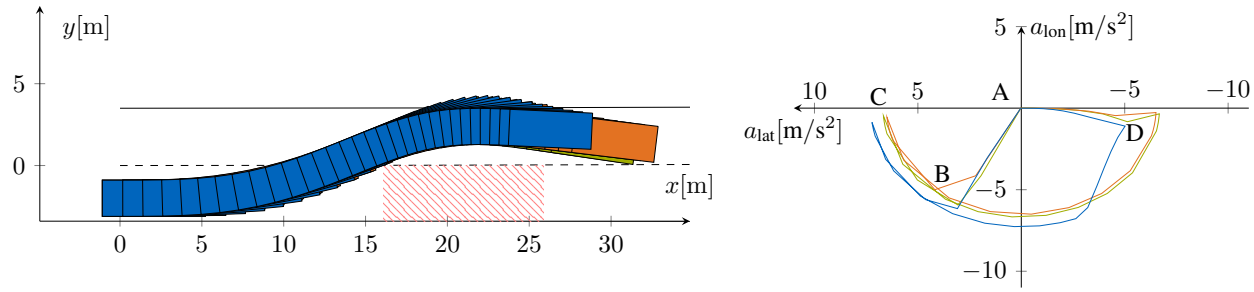

Fig. 2. Evasion trajectories with an initial velocity of 15m/s and static obstacle (hatched area). Left: top-down view, right: traces of longitudinal and lateral acceleration. OCP variants: max-norm of acceleration with nonlinear tire (green), linear tire (orange), maximum dynamics without input constraints (blue).

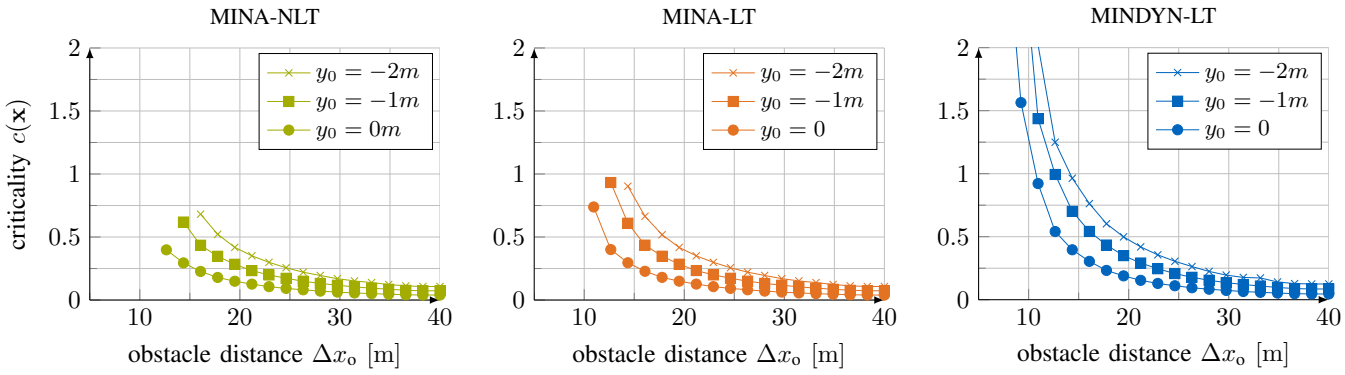

Fig. 3. Criticality labels for a standing obstacle at varying distances Δx_o and varying lateral offsets y for an initial velocity of $v_0 = 15\mathrm{m/s}$.

REFERENCES

[1] M. Distner, M. Bengtsson, T. Broberg, and L. Jakobsson, "City safety – a system addressing rear-end collisions at low speeds," in *Proc. Int. Tech. Conf. Enhanced Safety Veh., ESV*, no. 09-0371, 2009.

[2] A. Eidehall, J. Pohl, F. Gustafsson, and J. Ekmark, "Toward autonomous collision avoidance by steering," *IEEE Trans. Intell. Transp. Syst.*, vol. 8, no. 1, pp. 84–94, March 2007.

[3] S. C. Peters, "Optimal planning and control for hazard avoidance of front-wheel steered ground vehicles," Ph.D. dissertation, Massachusetts Institute of Technology, 2012.

[4] W. Wachenfeld and H. Winner, "Die freigabe des autonomen fahrens," in *Autonomes Fahren*, M. Maurer, J. C. Gerdes, B. Lenz, and H. Winner, Eds. Springer Berlin Heidelberg, 2015, pp. 439–464.

[5] J. Hillenbrand, A. Spieker, and K. Kroschel, "A multilevel collision mitigation approach – its situation assessment, decision making, and performance tradeoffs," *IEEE Trans. Intell. Transp. Syst.*, vol. 7, no. 4, pp. 528–540, Dec 2006.

[6] L. Yang, J. H. Yang, E. Feron, and V. Kulkarni, "Development of a performance-based approach for a rear-end collision warning and avoidance system for automobiles," in *IEEE Intell. Veh. Symp.*, June 2003, pp. 316–321.

[7] K. Lee and H. Peng, "Evaluation of automotive forward collision warning and collision avoidance algorithms," *Vehicle System Dynamics*, vol. 43, no. 10, pp. 735–751, 2005.

[8] J. Rohde, J. E. Stellet, H. Mielenz, and J. Zollner, "Model-based derivation of perception accuracy requirements for vehicle localization in urban environments," in *Intelligent Transportation Systems (ITSC), 2015 IEEE 18th International Conference on*, Sept 2015, pp. 712–718.

[9] M. Botsch and J. A. Nossek, "Feature selection for change detection in multivariate time-series," in *IEEE Symp. Computational Intell. Data Mining, CIDM*, March 2007, pp. 590–597.

[10] S. Herrmann, W. Utschick, M. Botsch, and F. Keck, "Supervised learning via optimal control labeling for criticality classification in vehicle active safety," in *Intelligent Transportation Systems (ITSC), 2015 IEEE 18th International Conference on*, Sept 2015, pp. 2024–2031.

[11] S. Karrenberg, "Zur Erkennung unvermeidbarer Kollisionen von Kraftfahrzeugen mit Hilfe von Stellvertretertrajektorien," Ph.D. dissertation, Technische Universität Braunschweig, 2008.

[12] I. Xausa, R. Baier, M. Gerdts, M. Gonter, and C. Wegwerth, "Avoidance trajectories for driver assistance systems via solvers for optimal control problems," in *Int. Symp. Math. Theory Networks Syst.*, 2012.

[13] T. Dirndorfer, M. Botsch, and A. Knoll, "Model-based analysis of sensor-noise in predictive passive safety algorithms," in *Proc. Int. Tech. Conf. Enhanced Safety Veh., ESV*, 2011.

[14] E. Bakker, L. Nyborg, and H. B. Pacejka, "Tyre modelling for use in vehicle dynamics studies," SAE Technical Paper, Tech. Rep., 1987.

[15] B. Johansson and M. Gafvert, "Untripped suv rollover detection and prevention," in *Decision and Control, 2004. CDC. 43rd IEEE Conference on*, vol. 5, Dec 2004, pp. 5461–5466 Vol.5.

[16] M. Brännström, E. Coelingh, and J. Sjöberg, "Decision-making on when to brake and when to steer to avoid a collision," *Int. J. Veh. Safety*, vol. 7, no. 1, pp. 87–106, Jan. 2014.

[17] H. G. Bock and K.-J. Plitt, "A multiple shooting algorithm for direct solution of optimal control problems," in *Proc. IFAC World Congr. Budapest*, Proceedings 9th IFAC World Congress Budapest. Pergamon Press, 1984, pp. 242–247. [Online]. Available: http://www.iwr.uni-heidelberg.de/groups/agbock/FILES/Bock1984.pdf

[18] J. Andersson, J. Akesson, and M. Diehl, "Casadi: A symbolic package for automatic differentiation and optimal control," in *Recent Advances in Algorithmic Differentiation*, ser. Lecture Notes in Computational Science and Engineering, S. Forth, P. Hovland, E. Phipps, J. Utke, and A. Walther, Eds. Springer, 2012, vol. 87, pp. 297–307.

[19] A. Wächter and L. T. Biegler, "On the implementation of an interior-point filter line-search algorithm for large-scale nonlinear programming," *Math. Programming*, vol. 106, no. 1, pp. 25–57, 2006.

[20] A. Berthelot, A. Tamke, T. Dang, and G. Breuel, "Handling uncertainties in criticality assessment," in *Intelligent Vehicles Symposium (IV), 2011 IEEE*, June 2011, pp. 571–576.